Zika virus infection preferentially counterbalances human peripheral monocyte and/or NK-cell activity

Fok-Moon Lum[1], David Lee[2], Tze-Kwang Chua[1], Jeslin J.L. Tan[1], Cheryl Y.P. Lee[1,3], Xuan Liu[4,5], Yongxiang Fang[4], Bernett Lee[1], Wearn-Xin Yee[1], Natasha Y. Rickett[5,6], Po-Ying Chia[7], Vanessa Lim[7], Yee-Sin Leo[7,8,9], David A. Matthews[2], Julian A. Hiscox[1,5,6]*, Lisa F.P. Ng[1,5,6,10]*

[1]Singapore Immunology Network, Agency for Science, Technology and Research (A*STAR), Singapore 138648, Singapore.

[2]School of Cellular and Molecular Medicine, University of Bristol, Bristol BS8 1TD, UK.

[3]NUS Graduate School for Integrative Sciences and Engineering, National University of Singapore, Singapore 117456, Singapore.

[4]Centre for Genomic Research, Institute of Integrative Biology, University of Liverpool, Liverpool L69 7ZB, UK.

[5]National Institute of Health Research, Health Protection Research Unit In Emerging and Zoonotic Infections, University of Liverpool, Liverpool L69 3GL, UK.

[6]Institute of Infection and Global Health, University of Liverpool, Liverpool L69 7BE, UK.

[7]Communicable Diseases Centre, Institute of Infectious Diseases and Epidemiology, Tan Tock Seng Hospital, Singapore 308433, Singapore.

[8]Lee Kong Chian School of Medicine, Nanyang Technological University, Singapore 636921, Singapore.

[9]Saw Swee Hock School of Public Health, National University of Singapore, Singapore 117549, Singapore.

[10]Department of Biochemistry, Yong Loo Lin School of Medicine, National University of Singapore, Singapore 117597, Singapore.

Correspondence: Prof Lisa F.P. Ng (lisa_ng@immunol.a-star.edu.sg); Prof Julian A. Hiscox (Julian.Hiscox@liverpool.ac.uk)

Abstract: 172 words

Main text: 6024 words

Inserts: 7 Figures and 2 Tables

Abstract

Zika virus (ZIKV) has re-emerged in the population and caused unprecedented global outbreaks. Here, the transcriptomic consequences of ZIKV infection were studied systematically firstly in human peripheral blood $CD14^+$ monocytes and monocyte-derived macrophages with high density RNA-sequencing. Analyses of the ZIKV genome revealed that the virus underwent genetic diversification and differential mRNA abundance was found in host cells during infection. Notably, there was a significant change in the cellular response with crosstalk between monocytes and natural killer (NK) cells as one of the highly identified pathway. Immune-phenotyping of peripheral blood from ZIKV-infected patients further confirmed the activation of NK cells during acute infection. ZIKV infection in peripheral blood cells isolated from healthy donors led to the induction of IFNγ and CD107a — two key markers of NK-cell function. Depletion of $CD14^+$ monocytes from peripheral blood resulted in a reduction of these markers and reduced priming of NK cells during infection. This was complemented by the immunoproteomic changes observed. Mechanistically, ZIKV infection preferentially counterbalances monocyte and/or NK-cell activity, with implications for targeted cytokine immunotherapies.

Introduction

Zika virus (ZIKV) gained global attention in 2015-2016 when the virus suddenly re-emerged in the human population and caused major viral outbreaks across the world with a large disease burden (1). Although ZIKV has been causing sporadic outbreaks since it was first reported in Uganda >60 years ago (2), very little is known about the biology of the virus and the host response to infection. ZIKV is an arthropod-borne flavivirus that causes Zika fever — a disease that for the majority of patients has little or no symptoms (3). However, in severe cases, ZIKV infection may be responsible for neurological complications such as Guillain Barré Syndrome (GBS) in adults (4) and congenital fetal growth-associated anomalies in newborns (5). The host response to ZIKV infection may be one of the main drivers of the different disease phenotypes.

Recent studies have established that ZIKV can infect peripheral blood monocytes (6-9). However, despite ongoing intensive investigative efforts to understand ZIKV-related neuropathogenesis, knowledge regarding the mechanisms of ZIKV infection in peripheral immune cells is lacking. Given that ZIKV is transmitted into the dermis via the bite from a virus-infected mosquito, monocytes would be one of the first immune cells in the blood to interact with the virus when it reaches the circulatory system. Therefore, the interplay between ZIKV and monocytes will be crucial in determining the outcome of infection (10).

This study focused on characterising the primary *ex vivo* response of human donor blood monocytes and monocyte-derived macrophages (MDMs) to ZIKV infection. Systematically, RNA-sequencing (RNA-seq) was

first used to identify and quantify the abundance of host messenger RNA (mRNA) and characterise viral RNA. This information was subsequently used to map the host response to ZIKV infection in the two different *ex vivo* cell types. These data also provided insights into the potential adaptation of the virus during viral replication in these cells. Immune-phenotyping of peripheral blood cells isolated from patients infected with ZIKV independently was executed to validate the predictions obtained from the differential gene expression analysis. Depletion of $CD14^{+}$ monocytes in peripheral blood was then performed *ex vivo* to functionally understand the crosstalk between monocytes and priming of NK cells during ZIKV infection. Lastly, a multiplex assay was carried out to further understand host cell immunoproteomic changes during ZIKV infection. To our knowledge, this study is the first large-scale systematic investigation into the host cellular response to ZIKV infection in biologically relevant cells. This global analysis of the host immune response provides a novel understanding of the pathobiology of the virus, leading to the possibility of targeted therapeutic interventions in severe cases.

Results

ZIKV targets human peripheral blood monocytes and macrophages. $CD14^+$ monocytes have been reported to be the main targets of ZIKV during infection (6-9). In this study, human primary $CD14^+$ monocytes were first isolated from fresh peripheral blood mononuclear cells (PBMCs) to enrich this cell type to >90% of the total cell population (Figure 1A). In addition, isolated monocytes from the same donors were differentiated into monocytes-derived macrophages (MDMs) over 5 days (Figure 1B). Purified cells were then infected *ex vivo* with ZIKV and their permissiveness to ZIKV infection and growth was determined at 24 and 72 hours post-infection (hpi) (Figure 1A). The 24 hpi time point was chosen to represent the acute infection phase and the 72 hpi time point a stage by which a substantial host-virus interaction would have taken place (11). Data obtained showed that ZIKV infection of MDMs was more significant than infection of monocytes in all five donors (~40% compared to ~20% at 72 hpi, respectively) (Figure 1C). A decrease in viral load was observed in the virus-infected MDMs between the two time points, whereas the viral load remained consistent in infected monocytes over time (Figure 1D).

In parallel, virus infection in PBMCs obtained from four healthy human volunteers also showed that $CD14^+$ monocytes were the main immune subsets infected (Supplemental Figure 1).

Genome variation in ZIKV during infection of the peripheral blood. In order to compare the amount of virus between the different cell types and determine whether ZIKV underwent genetic diversification during infection,

viral sequence reads were mapped and compared to that of the progenitor virus stock (PF/ZIKV/HPF/2013). These data indicated that for MDMs, 4.53% and 0.43% of total sequence reads mapped to the ZIKV genome at 24 hpi and 72 hpi, respectively. While 24% and 0.8% of sequence reads generated from monocytes mapped to the ZIKV genome at 24 hpi and 72 hpi respectively. These observations are consistent with ZIKV viral load analysis, where higher levels of viral RNA were detected in MDMs (Figure 1).

Due to the inherent error-prone nature of viral RNA replication, nucleotide variants may become established in the viral genome during ZIKV infection in different cell types. To investigate this hypothesis, consensus genome information for each sample and the frequency of minor variants at each nucleotide position in the progenitor stock was determined and compared to the genome of virus present in the infected samples utilizing previously developed workflows (12,13). The ZIKV consensus genome sequence derived from the progenitor stock was 10,570 nucleotides in length and contained minor variants (as a measure of quasi-species) spread throughout the genome (Figure 2A). Of the 11 valid consensus sequences derived from the virus-infected samples, the virus recovered in cells from five donors (D1-D5) had the same consensus sequence as the input stock (PF/ZIKV/HPF/2013). However, some donor samples contained viral genomes that had additional nucleotide differences at six different positions (Table 1). These nucleotide differences (Table 1) were visualized as a maximum likelihood phylogenetic tree, where the input stock was used as the reference sample (Figure 2B). There were only eight high frequency transition mutations to choose from ($\log_{10}8 = 0.9$, see Figure 2A), increasing the

likelihood of these changes appearing several times. Of these eight transition mutations, six appeared as major variants and thus changed the overall consensus sequence. The nucleotide positions of these six transition mutations (Table 2) indicated that all the changes in the consensus sequence were already present at relatively high frequency as minor variants in the input stock and were subsequently amplified during viral replication. Changes at nucleotide positions 2,815 and 4,211 were the most common, being found in ~35% reads mapping to the virus genome. Had these changes been found in ≥50% reads, they would have been classified as major variants and thus changed the consensus sequence (Table 2).

Transcriptomic profiling reveals key cellular responses to ZIKV infection. RNA-seq was used to identify and quantify global mRNA abundance in ZIKV-infected peripheral monocytes and MDMs at 24 and 72 hpi. mRNA purified from 27 samples showed no signs of degradation and had sufficient read depth for inclusion in the analyses (Supplemental Figure 2A). For monocytes, mock and ZIKV-infected cells at both 24 and 72 hpi exhibited minimal changes in host transcript abundance. For MDMs, the abundance of transcripts that mapped to 1,736 and 545 genes at 24 and 72 hpi respectively, were significantly different (FDR < 0.05) between the mock and ZIKV-infected samples (Supplemental Figure 2B).

Ingenuity Pathway Analysis (IPA) was used to interrogate and group the differentially expressed genes into functional pathways (Figure 3A). A total of 169 pathways were identified, of which 27 were common in ZIKV-infected MDMs at 24 and 72 hpi. A further 106 pathways were unique to samples at 24

hpi (Supplemental Table 1), and 36 pathways were unique to samples at 72 hpi (Supplemental Table 2). This analysis found that genes associated with the interferon response were significantly upregulated at both time-points. In addition, signalling pathways involved in the pathogenesis of multiple sclerosis, and key pathways involved in monocyte-derived dendritic cell (moDCs) and NK cell processes were also shared between the two time points (Figure 3A). Overall, the top three common pathways activated in MDMs were interferon signalling, multiple sclerosis pathogenic pathways and crosstalk pathways between moDCs and NK cells (Figure 3A). The specific genes with the most abundant transcripts within these three pathways were analyzed, and when compared to the mock-infected controls were all increased in abundance after ZIKV infection (Figure 3B).

Virus-infected MDMs exhibit reduced cellular responsiveness. Transcriptomic profiles of various ZIKV-infected MDMs were compared to evaluate the transition of the cellular host response over the course of ZIKV infection. The percentage overlap of the identified transcripts between ZIKV-infected MDMs was assessed at 24 hpi and 72 hpi within the three targeted pathways described above (Figure 4). Interestingly, the percentage of overlapping transcripts identified at 72 hpi was lower for all three pathways, which may reveal a lower activation status of these pathways at this stage of the infection. The identification of different transcripts associated with 72 hpi may indicate the different signalling cascades present or activation status of these cells (Figure 4A). Global assessment of all identified transcripts revealed that transcripts mapping to 251 genes were in fact present in virus-

198 infected MDMs at both time points. Transcripts that mapped to 1,485 genes
199 were specific to 24 hpi, of which 54.81% exhibited greater abundance
200 compared to the mock controls. By comparison, transcripts that mapped to
201 294 genes were unique to 72 hpi, with 63.36% of them having greater mRNA
202 abundance compared to the mock controls (Figure 4B). Within the 251
203 common genes, transcripts mapping to 218 genes had a greater fold-change
204 value compared to the mock-infected controls, indicating that these transcripts
205 were increased in abundance in all ZIKV-infected MDMs. Further inquiry of
206 these transcripts revealed that 60.1% of them were greater in abundance at
207 72 hpi compared to 24 hpi. Likewise, of the remaining transcripts that mapped
208 to 33 genes and showed decreased abundance, 84.85% were further reduced
209 at 72 hpi.

210

211 **NK cells are activated in ZIKV-infected patients.** IPA predicted robust
212 crosstalk between NK cells and moDCs in peripheral blood upon *ex vivo*
213 ZIKV infection (Figure 3-4). The IPA prediction that NK cells were activated
214 in the peripheral blood of ZIKV-infected patients was, therefore,
215 investigated by comprehensive immune-phenotyping of blood samples
216 taken from ZIKV-infected patients. These patients were recruited from the
217 first endemic ZIKV outbreak in Singapore in 2016 (7,14). Blood aliquots
218 were obtained from ZIKV-infected patients (n=9) during the acute disease
219 phase (between 1 and 7 days post-illness-onset), and were subjected to a
220 whole blood staining protocol that targeted $CD56^{+}$ cells, predominantly NK
221 cells (15) (Figure 5A). Blood from healthy donors (n=5) was collected and
222 processed in parallel as a control group. Gated cells were further grouped

with the C-type lectin receptor CD94, giving three $CD56^{+}$ populations: $CD56^{bright}CD94^{hi}$, $CD56^{dim}CD94^{hi}$ and $CD56^{dim}CD94^{lo}$ (16). The activation status of these populations was then assessed based on the percentage of each subset expressing CD16 and CD69 (Figure 5B). A higher level of CD16 was observed across all $CD56^{+}$ subsets in ZIKV-infected patients compared to the healthy controls. A higher percentage of the subsets also expressed CD69 — a known cellular activation marker (17).

$CD14^{+}$ monocytes prime NK-cell activity during ZIKV infection. Given that peripheral NK cells were activated in ZIKV-infected patients and monocytes are precursors of MDMs, the functional relationship between monocytes and NK cells were assessed. $CD14^{+}$ monocytes were depleted from human primary PBMCs, with an average efficiency of >95% (Supplemental Figure 3). Lipopolysaccharide (LPS; 10ng/ml) was used as a positive control to simulate priming of NK cells by monocytes (18). A significant reduction in the activity of NK cells was observed when CD14-depleted PBMCs were stimulated with LPS compared to LPS stimulation of PBMCs containing $CD14^{+}$ monocytes (Supplemental Figure 4). This effect was evidenced by the reduced levels of the surface markers CD69, CD107a and intracellular IFNγ in depleted cells, verifying that this approach was an efficient strategy for investigating priming of NK cells by $CD14^{+}$ monocytes

PBMCs were then isolated from seven healthy donors and subjected to CD14-depletion before being either infected with ZIKV or stimulated with LPS in parallel to serve as a control to determine activation of NK cells. ZIKV infection in non-depleted PBMCs resulted in high levels of CD107a and IFNγ

(Figure 6A) in $CD56^{+}CD94^{+}$ NK cells (Supplemental Figure 5) at 36 hpi — an optimal time-point to detect NK-cell priming (19). The opposite effect, however, was observed in ZIKV-infected PBMCs depleted of $CD14^{+}$ monocytes as the levels of both CD107a and IFNγ were significantly reduced (Figure 6B). The levels of CD107a and IFNγ remained high at 72 hpi in non-depleted infected PBMCs compared to depleted infected PBMCs (Supplemental Figure 6). Interestingly, although monocyte depletion did not affect the expression of NK-cell activation receptors NKG2A or NKG2D, a general reduction in NKG2D-expressing NK cells was observed during ZIKV infection (Supplemental Figure 7A and 7B). Surprisingly, the activation marker CD69 was not increased upon ZIKV infection in this study (Supplemental Figure 7C and EV7D). ZIKV viral load was comparable between both conditions (Figure 6C).

To delve further into the mechanism, the profile of secreted immune mediators from ZIKV-infected PBMCs was quantified using a 45-plex microbead-based immunoassay (20). Levels of 11 mediators were significantly affected by the depletion of $CD14^{+}$ monocytes (Figure 7A and Supplemental Figure 8A), while 8 mediators were affected upon ZIKV infection (Supplemental Figure 8B). Interestingly, depletion of $CD14^{+}$ monocytes and ZIKV infection did not affect the levels of EGF, IL-9, IL-17A, MIP-1α and MIP-1β (Supplemental Figure 8C). The effect of $CD14^{+}$ monocytes depletion was observed in the levels of SCF and TNFα only after ZIKV infection (Supplemental Figure 8D). Importantly, levels of MCP-1, IL1RA and VEGF-A were affected by both $CD14^{+}$ monocytes depletion and ZIKV infection (Figure 7B). To further investigate the capacity of the cytokine

milieus in priming NK cells, freshly isolated human primary PBMCs were then treated with the same culture supernatants from ZIKV-infected PBMCs and $CD14^+$ monocytes-depleted PBMCs. Stimulation with culture supernatant from ZIKV-infected non-depleted PBMCs led to slightly more cell death (Supplemental Figure 9A) accompanied by a significant upregulation in expression of CD107a, IFNγ and NKG2D in the $CD94^+CD56^+$ NK cells (Figure 7C and Supplemental Figure 9B), confirming the importance of monocytes in NK-cell priming during ZIKV infection. To rule out priming of NK cells by viruses present in the culture supernatant, a UV-treatment procedure was performed to inactivate the virus, prior to the stimulation assay. Expectedly, while UV-inactivation successfully inactivated ZIKV (Supplemental Figure 10A), it also affected the quality of the cytokines and led to reduced priming of NK cells (Supplemental Figure 10B).

Discussion

Myeloid cells are targets of active ZIKV infection (6-9,21-23) and can elicit immune responses with detrimental outcomes (6,8). Both monocytes and macrophages exhibit extensive heterogeneity (24,25). While it is difficult to obtain tissue-resident macrophages for experimental purposes, human blood is a readily accessible, valuable source of these cells. Transcriptomic profiling of *ex vivo* human blood monocytes and MDMs has revealed marked differences between these cell types (26,27). In this study, human primary monocytes were naturally differentiated into MDMs without any bias for an M1 or M2 macrophage phenotype (28). Given that these cells are targets of ZIKV infection (8), investigations into their cellular immune responses during infection will open avenues to exploit their function for therapeutic benefits.

The level of ZIKV infection (as assessed by the amount of ZIKV antigen and genome copy number) was higher in MDMs than monocytes, which corroborates previous observations (8). Transcriptomic differences between monocytes and MDMs (26,27) would be a plausible explanation for the differential susceptibility of these cells to ZIKV infection. It is also noteworthy that higher ZIKV infection levels were found in purified primary cell populations compared to PBMCs, perhaps due to the presence of other immune subsets in PBMCs that may dampen the overall infection level. ZIKV RNA was detected at the two time-points, 24 and 72 hpi and the virus was present as quasi-species post-infection in human primary myeloid cells. The virus consensus sequence and minor variant mapping revealed an over-representation of transition mutations at highly variable nucleotide

positions in the sequence reads. The proportion of these minor variants indicated a shift towards becoming major variants. A recent study that sequenced ZIKV genomes isolated from infected patients provided important information pertaining to ZIKV transmission (29). These data highlighted the degree of divergence in sequenced genomes and placed further emphasis on understanding virus evolution and transmission effectiveness (30). As not all recovered ZIKV RNA samples contained the same mutations, it will be interesting to determine how different host immune responses can lead to ZIKV quasi-species that acquire different combinations of mutations.

ZIKV infection led to the differential abundance of host transcripts mapping to numerous cellular genes in MDMs but not in monocytes, likely due to higher levels of infection observed in MDMs. Furthermore, it has been reported that different donors could account for significant differences in cellular responses (31,32). However, this differential effect does not necessary signify that ZIKV-infected monocytes do not elicit any cellular response to infection, but rather the differences were not measurable by RNA-seq at the read depths used in this analysis. In fact, transcript abundance of numerous genes were different between the mock and ZIKV-infected monocytes, just that the statistical threshold of FDR < 0.05 was not reached and was thus excluded from further analyses. Using IPA data mining, these differentially expressed genes were involved in 133 and 63 canonical cellular pathways (27 of them being shared) in MDMs at 24 and 72 hpi, respectively. The lower number of cellular pathways identified in ZIKV-infected MDMs at the later 72 hpi time-point suggests that certain cellular

functions may be shut down post-infection (33). This effect could signify: (1) that the host cells conserve energy to focus only on essential pathways for survival; and/or (2) the host cells have succumbed to ZIKV infection, which leads to transcriptional shutdown in host cells.

Unsurprisingly, the IFN response was the most highly expressed signalling pathway of these common pathways at both time-points because of virus trigger (34). This observation was further complemented by the presence of few other IFN-related pathways. Observations were found for the next two most expressed pathways — pathogenesis of multiple sclerosis and crosstalk between NK cells moDCs cells — both of which involve NK cells. Although ZIKV infection has not been previously associated with multiple sclerosis due to the relatively new disease spectrum, other viral infections such as Epstein-Barr virus (35) and measles virus (36) have been linked.

CXCL9, CXCL10, CXCL11 and CCL5 (identified as the top genes in the pathway) are known chemokines to stimulate NK-cell activation (37,38). The increased transcript abundance of these immune mediators, coupled with others such as IL-15, is a strong indication that ZIKV-infected macrophages are primed to “communicate” with NK cells. Other recent studies have also provided evidence of cross-talk between macrophages and NK cells (18). The increased abundance of TNFSF10 and FAS transcripts in ZIKV-infected MDMs, could indicate priming of NK-cell mediated apoptosis (39). Interestingly, levels of typical NK cell-activating cytokines, such as IL-12 (40,41) and IL-18 (42,43) were not differentially expressed in this study. However, mRNA levels of IL-23 and IL-27, two

cytokines belonging to the family of IL-12 (44) with roles in NK-cell activation (45,46) were increased.

Immune-phenotyping of whole blood samples from ZIKV-infected patients revealed the presence of $CD69^{+}CD56^{+}$ immune cells (predominantly the $CD56^{+}$ NK cells) (15), suggesting the possible priming of NK cells in ZIKV infection. The involvement of NK cells was thus explored *ex vivo* in human primary PBMCs. Interestingly, *ex vivo* culture alone led to an increase in the basal expression level of CD69 in $CD56^{+}CD94^{+}$ NK cells, as previously reported (47). Furthermore, ZIKV infection resulted in reduced levels of CD69, which is a phenomenon also reported for the flavivirus tick-borne encephalitis virus infection in healthy donor NK cells (48). Moreover, NK cells behave differently *ex vivo* and *in vivo* (49), which may explain the different levels of CD69 detected in patients and in *ex vivo* ZIKV-infected NK cells. It was also reported in CD69-deficient mice that the activity of NK cells remains functional (50). High levels of key NK activation markers, including the degranulation marker CD107a and intracellular cytokine IFNγ indicate the higher activation status of NK cells. The activity of NK cells was directly dependent on the presence of $CD14^{+}$ monocytes. ZIKV infection of PBMCs depleted of $CD14^{+}$ monocytes significantly down-regulated the expression of the various NK-cell markers, demonstrating the functional role of monocytes as one of the key players for NK-cell stimulation. The data presented in this study are further supported by a recent publication in which ZIKV patients had high levels of IL-18, TNFα and IFNγ (20) — immune mediators associated with NK-cell function. The usage of SJL mice, which lack NK cells (51), as a model of ZIKV infection also suggested

386 a protective role for these immune cell given that these animals succumbed
387 to cortical malformations (52). Likewise, NK-cell-mediated immune
388 response was significantly increased in healthy volunteers receiving a
389 vaccination for the closely related yellow fever virus (53).

390 Interestingly, multiplex quantification of secreted immune mediators
391 from *ex vivo* ZIKV-infected PBMCs provided an alternate perspective. IL-18
392 and IFNγ, two NK-cell related cytokines, were below detection limit.
393 However, freshly isolated PBMCs stimulated with culture supernatants from
394 ZIKV-infected PBMCs resulted in increased priming of NK cells, clearly
395 indicating that the concoction of immune mediators are capable in driving
396 NK-cell activation.

397 Nonetheless, the, depletion of $CD14^+$ monocytes would abrogate this
398 activation as observed by the low levels of MCP-1, IL-1RA, VEGF-A,
399 Eotaxin, GROα, IFNα SDF-1α, IP-10, IL-6, IL-1α, IL-1β, IL-8, IL-21 and IL-
400 10. The reduced levels of MCP-1 could also have a detrimental effect on
401 NK-cell recruitment and priming (37,54), although MCP-1 and VEGF-A
402 have been reported to drive the production of each other (55-57). The high
403 levels of secreted IL1RA from ZIKV-infected PBMCs could also have
404 participated in the increased priming of NK cells, as IL1RA is known to
405 potentiate the effect of IL-2 stimulation of NK cells (58). Thus, the loss of
406 detectable IL-2 after ZIKV infection in CD14-depleted PBMCs would further
407 dwindle NK-cell priming. The presence of other immune mediators such as
408 IL-6, IL-8, IL-10 and IP-10, SDF-1α, GROα, IL-1α and IL-1β in ZIKV-
409 infected non-depleted PBMCs would further provide an inflammatory
410 condition for cellular activation. While the levels of these immune mediators

411 have been reported to be high in ZIKV patients (20), IL-10 and IP-10 have
412 been demonstrated to contribute to cytolysis and activation of NK cells
413 (37,59). Levels of LIF (60), IL-22 (61) and IL-31 (62) were high upon ZIKV
414 infection, indicating their roles in regulating T cells during ZIKV infection
415 (63). T cells can regulate NK-cell activity (64) and monocytes could
416 indirectly mediate NK-cells functions through the T lymphocytes.

417 To conclude, through a systematic investigative workflow combining
418 approaches exploring host cell transcriptomes and immunoproteomes, it was
419 demonstrated that monocytes and macrophages do not act alone, but in
420 conjunction with other immune cells to orchestrate a series of host immune
421 response and drive disease progression. As such, a comprehensive
422 understanding of immune-cell interaction will have important clinical
423 implications for the design of novel therapeutics that can either dampen down
424 or enhance a response as appropriate.

425 **Materials and Methods**

426 **Ethics approval and consent to participate.** Whole blood samples were
427 collected from ZIKV-infected patients who were referred to the Communicable
428 Disease Centre, Tan Tock Seng Hospital, Singapore. Blood was obtained
429 from patients who provided written informed consent. The study protocol was
430 approved by the SingHealth Centralized Institutional Review Board (CIRB
431 Ref: 2016/2219). Blood samples were collected from healthy donors with
432 written consent in accordance with guidelines from the Health Sciences
433 Authority of Singapore (study approval number: NUS IRB: 10-250).

434

435 **Patient whole blood samples.** This study utilized whole blood samples
436 obtained from patients admitted to the Communicable Disease Centre at Tan
437 Tock Seng Hospital, Singapore from 27 August to 18 October 2016. Samples
438 included in this study were collected during the acute phase (1-7 pio) of ZIKV
439 infection. These patients were confirmed to be infected with ZIKV by reverse-
440 transcription polymerase chain reaction (RT-PCR) performed on serum and
441 urine samples obtained during their first visit to the clinic. Whole blood
442 samples were collected in EDTA Vacutainer tubes (Becton Dickinson). Whole
443 blood samples were also obtained from healthy volunteers as controls, which
444 were confirmed to be negative for ZIKV RNA by RT-PCR.

445

446 **Virus preparation.** The ZIKV strain (accession KJ776791) used in this study
447 was originally isolated from the French Polynesia outbreak in 2013 (65). The
448 virus was propagated as previously described (8). Briefly, the virus was
449 propagated by multiple passages in Vero-E6 cells (ATCC*;* CRL-1587) and

pre-cleared by centrifugation before storing at -80^{o}C. The virus titre was determined using standard plaque assays with Vero-E6 cells. Vero-E6 cells were regularly tested for mycoplasma contamination and were grown and passaged in Dulbecco's Modified Eagle Medium (DMEM; HyClone) supplemented with 10% (vol/vol) FBS. UV-inactivation of ZIKV was performed with the CL-1000 UV cross-linker (UVP) at intensity of 100mJ/cm^2 for 10 minutes.

Isolation and depletion of monocytes from human PBMCs. Monocytes were prepared from fresh human PBMCs as previously described (8) and by gradient centrifugation using Ficoll-Paque density gradient media (GE Healthcare). Subsequently, monocytes were isolated using an indirect magnetic labelling system (Monocyte Isolation Kit II, Miltenyi Biotec). A direct magnetic labelling system (Human CD14$^+$ monocytes isolation kit 2, STEMCELL) was used for depletion of monocytes from PBMCs. The manufacturers' protocols were strictly adhered to for these procedures.

Differentiation of monocytes into MDMs. Isolated monocytes were differentiated into MDMs by plating in complete Iscove Modified Dulbecco's Medium (IMDM) (Hyclone) supplemented with 10% (vol/vol) heat-inactivated human serum (HS) (Sigma-Aldrich), which was replaced every 2 days. ZIKV infections were performed on monocytes and MDMs 5 days later, as described below.

Virus infection. ZIKV infections were performed at multiplicity of infection (MOI) 10. Each infection mix consisted of a virus suspension prepared in serum-free IMDM (Hyclone). The cells were incubated with the infection mix at 37^{o}C and allowed to adsorb for 2 h with intermittent shaking before the virus inoculum was removed and replaced with complete IMDM supplemented with 10% (vol/vol) HS (Sigma-Aldrich). Cells were incubated at 37^{o}C until harvesting at 24 and 72 hpi. The harvested cells for downstream total RNA isolation were stored at -80^{o}C. A total of 140 µl of the infected cell suspension was used to quantify the viral load. For assessment of monocyte function in NK-cell activation during ZIKV infection, total human PBMCs and donor-corresponding CD14-depleted PBMCs were infected with ZIKV at MOI 10. In parallel, both PBMC fractions were stimulated with 10ng/ml lipopolysaccharide (LPS; Sigma) as a positive control to measure NK-cell activation. Cells were subsequently treated with 1X Brefeldin (eBioscience) and stained with CD107a (BD Pharmingen) 6 h before harvesting at 36 hpi. The viral load was quantified from 140 µl of the infected cell suspension. Negative controls were cells undergoing the same infection conditions in the absence of infectious ZIKV particles. These controls are referred to as mock-infected samples.

PBMCs stimulation assay. Fresh PBMCs were isolated as described above and subjected to stimulation with ZIKV-infected culture supernatants in a final ration of 1:10 in fresh IMDM (Hyclone) supplement with 10% (vol/vol) of HS (Sigma-Aldrich). Cells were subsequently treated with 1X Brefeldin

(eBioscience) and stained with CD107a (BD Pharmingen) 6 h before harvesting at 36 h for downstream antibodies staining.

Viral RNA extraction and viral load analysis. Viral RNA was extracted using a QIAamp® Viral RNA Mini Kit (QIAGEN), according to manufacturer's instructions. Quantification of ZIKV NS5 RNA was determined by quantitative real time-PCR (qRT-PCR) TaqMan assay (66) using a QuantiTect® Probe RT-PCR Kit (QIAGEN) in a 12.5 µl reaction volume. All reactions were performed on a 7900HT Fast Real-Time PCR System machine (Applied Biosciences).

Total RNA extraction. Total RNA was extracted using an RNeasy Mini Kit (QIAGEN) according to the manufacturer's instructions. The extracted total RNA was quantified on a Nanodrop 1000 spectrophotometer (Thermo Fisher Scientific).

Flow cytometry and antibodies. Detection of ZIKV antigen was carried out in a two-step indirect intracellular labelling process. Briefly, harvested cells were first fixed and permeabilized with FACS lysing solution (BD Biosciences) and FACS permeabilization solution 2 (BD Biosciences), respectively. Antigen staining was then performed with a flavivirus-specific mouse monoclonal antibody (clone 4G2) (Millipore) followed by secondary staining with a goat anti-mouse IgG $F(ab')_2$ antibody (Invitrogen). Cells were then specifically stained for the surface markers CD45 and CD14 (for ZIKV-infected monocytes and MDMs). Dead cells were excluded by staining with the

LIVE/DEAD Fixable Aqua Dead Cell Stain Kit (Life Technologies). For PBMCs, surface markers CD45, CD14, CD3, CD19 and CD56 were stained prior to intracellular staining (for ZIKV-infected PBMCs). For patient samples, 100 µl of whole blood was stained for the surface markers, CD45, CD56, CD94, CD16, CD69, CD107a, NKG2D and NKG2A. The stained cells were subsequently incubated with FACS lysing solution (BD Biosciences) to lyse the red blood cells. CD56+ cells were first identified and were subsequently further defined with the CD94 surface marker to give three other subsets - $CD56^{bright}CD94^{hi}$, $CD56^{dim}CD94^{hi}$ and $CD56^{dim}CD94^{lo}$ (16). To specifically assess NK-cell activity *ex vivo*, PBMC fractions were stained for CD107a and various lineage markers (CD3, CD19, CD20 and CD14) (15) in addition to the panel of antibodies used for patient whole blood staining. The usage of lineage markers excludes the presence of non-NK cells in the ensuing analysis. Stained PBMCS were fixed and permeabilized as described above before intracellular staining of ZIKV antigen and IFNγ.

All antibodies used were mouse anti-human and were obtained from BD Pharmingen (CD3, CD19, CD20, CD14, CD69, CD56, CD94, NKG2D, CD107a and IFNγ), Biolegend (CD16 and CD45) and Miltenyi Biotec (NKG2A). Data were acquired on a Fortessa flow cytometer (BD Biosciences) with BD FACSDiva™ software. Data analysis was performed using FlowJo version 9.3.2 software (Tree Star, Inc).

Cytokines quantification using microbead-based immunoassay and data analyses. Cytokine levels in supernatant obtained from mock and ZIKV-infected PBMCs were measured simultaneously using the ProcartaPlex™

548 immunoassay (Thermo Fisher Scientific) detecting for 45 secreted cytokines,
549 chemokines and growth factors including brain derived neurotropic factor
550 (BDNF); Eotaxin/CCL11; epidermal growth factor (EGF); fibroblast growth
551 factor 2 (FGF-2); granulocyte macrophage-colony stimulating factor (GM-
552 CSF); growth-related oncogene (GRO) alpha/CXCL1; hepatocyte growth
553 factor (HGF); nerve growth factor (67) beta; leukemia inhibitory factor (10);
554 interferon (IFN) alpha; IFN gamma; interleukin (IL)-1 beta; IL-1 alpha; IL-1RA;
555 IL-2; IL-4; IL-5; IL-6; IL-7; IL-8/CXCL8; IL-9; IL-10; IL-12p70; IL-13; IL-15; IL-
556 17A; IL-18; IL-21; IL-22; IL-23; IL-27; IL-31; interferon-gamma induced protein
557 (IP)-10/CXCL10; monocyte chemoattractant protein (MCP-1/CCL2);
558 macrophage inflammatory protein (MIP)-1 alpha/CCL3; MIP-1 beta/CCL4;
559 regulated on activation, normal T cell expressed and secreted
560 (RANTES)/CCL5; stromal cell-derived factor (SDF)-1 alpha/CXCL12; tumor
561 necrosis factor (TNF) alpha; TNF beta/LTA; Platelets-derived growth factor
562 (PDGF)-BB; placental growth factor (PLGF); stem cell factor (SCF); vascular
563 endothelial growth factor (VEGF)-A; VEGF-D. Preparation of samples,
564 reagents and immunoassay procedures were performed according to
565 manufacturers' instructions. Data were acquired using Luminex FlexMap 3D®
566 instrument (Millipore) and analyzed using Bio-plex Manager™ 6.0 software
567 (Bio-Rad) based on standard curves plotted through a five-parameter logistic
568 curve setting. Levels of BDNF, FGF-2, HGF, NGF, IFN gamma, IL-4, IL-5, IL-
569 7, IL-12p70, IL-13, IL-15, IL-18, RANTES, PDGF-BB, PLGF and VEGF-D
570 were below detection limit and excluded for further analysis. Hierarchical
571 clustering was done using TM4-MeV (http://mev.tm4.org/).
572

573 **RNA-seq and differential gene expression analysis.** The general approach
574 to RNA-seq and differential expression has been previously described
575 (10,68), and is detailed in brief below.
576
577 **RNA-seq.** RNA samples were treated with DNase using an Ambion Turbo
578 DNA-free Kit (Ambion), and then purified using Ampure XP beads
579 (Agencourt). The DNase-treated RNA (2 ug) underwent Ribozero treatment
580 using an Epicentre Ribo-Zero Gold Kit (Human/Rat/Mouse) (Epicentre) and
581 re-purified on Ampure XP beads. Successful RNA depletion was verified
582 using a Qubit (Thermo Fisher Scientific) and an Agilent 2100 Bioanalyzer
583 (Agilent) and all of the depleted RNA was used as input material for the
584 ScriptSeq v2 RNA-Seq Library Preparation protocol. RNA was amplified for
585 14 cycles and the libraries were purified on Ampure XP beads. Each library
586 was quantified using Qubit and the size distribution was assessed using the
587 AATI Fragment Analyser (Advanced Analytical). These final libraries were
588 pooled in equimolar amounts using the Qubit and Fragment Analyser data.
589 The quantity and quality of each pool was assessed by the Fragment
590 Analyser and subsequently by qPCR using the Illumina Library Quantification
591 Kit (KAPA Biosystems) on a Light Cycler LC480II (Roche) according to
592 manufacturer's instructions. The template DNA was denatured according to
593 the protocol described in the Illumina cBot User guide and loaded at 12 pM
594 concentration. Sequencing was carried out on three lanes of an Illumina
595 HiSeq 2500 with version 4 chemistry, generating 2 × 125 bp paired-end reads.
596

Bioinformatics Analysis. Briefly, base calling and de-multiplexing of indexed reads was performed using CASAVA version 1.8.2 (Illumina) to produce 30 samples from the five lanes of sequence data in fastq format. The raw fastq files were trimmed to remove the Illumina adapter sequences using Cutadapt version 1.2.1 (69). The option "-O 3" was set so that the 3' end of any read that matched the adapter sequence by ≥3 bp was removed. The reads were further trimmed to remove low-quality bases using Sickle version 1.200 with a minimum window quality score of 20. After trimming, reads <50 bp were removed. If both reads from a pair passed this filter, each read was included in the R1 (forward reads) or R2 (reverse reads) file. If only one read of a read pair passed this filter, it was included in the R0 (unpaired reads) file. The reference genome used for alignment was the human reference genome assembly GRCh38. The reference sequence was downloaded from the Ensembl ftp site (ftp://ftp.ensembl.org/pub/release77/fasta/homo_sapiens/dna/Homo_sapiens GRCh38.dna_sm.primary_assembly.fa.gz). The reference annotation was also downloaded from the Ensembl ftp site (ftp://ftp.ensembl.org/pub/release-77/gtf/homo_sapiens/Homo_sapiens.GRCh38.77.gtf.gz). The annotated file contained 63,152 genes. R1/R2 read pairs were mapped to the reference sequence using TopHat2 version 2.1.0 (70) that employs the mapper Bowtie2 version 2.0.10 (71).

Differential Gene Expression and Functional Analysis. Mapped reads were further analyzed using EdgeR version 3.3 (72) to calculate normalized counts per million (CPM), identify differentially expressed genes between

622 infected and mock-infected conditions, and compare infected conditions with
623 each other. Correlation and PCA analysis plots were created in RStudio.
624 Heat-maps were generated using GENE-E (Broad Institute;
625 https://software.broadinstitute.org/GENE-E/). IPA was used for gene ontology
626 and pathway analysis. The *P* value associated with each identified canonical
627 pathway was calculated by Fisher's Exact test (right-tailed). The presence of
628 the 27 common canonical pathways was illustrated in a heat-map generated
629 by hierarchical clustering using TM4-MeV (73).
630
631 **Identification of ZIKV variants.** Bowtie 2 (71) was used to determine the
632 mean sequence coverage. Here, 12 of the 41 samples (including the
633 inoculum) had a mean coverage >10 following alignment with the ZIKV
634 reference genome (accession KJ776791) used in this study. The frequencies
635 of minor variants were calculated using QuasiRecomb (74). Sequences of
636 individual viral proteins were compared to the protein databank using the
637 online NCBI Protein BLAST server
638 (https://blast.ncbi.nlm.nih.gov/Blast.cgi?PAGE=Proteins).
639

Author contributions

FML, DAM, JAH and LFPN designed the study. FML, DL, DAM, JAH and LFPN wrote the manuscript. FML, CTK, CLYP, JJLT, XL, WXY and YXF performed the experiments. FML, DL, XL, YXF, BL, NYR, DAM, JAH and LFPN analysed the data. All other authors were involved in sample collection, processing and analysis, and/or logistical support. All authors read and approved the final manuscript.

Acknowledgements

The authors would like to thank Siti Naqiah Amrun, Yiu-Wing Kam, Jonathan Cox, Yi-Hao Chan, Guillaume Carissimo, Farhana Abu Bakar, Nicholas Q.R. Kng, Kia-Joo Puan and Nurhashikin Binte Yusof from SIgN for their help in the processing of patient samples. The authors also thank Linda Kay Lee from the Communicable Diseases Centre and Ivy Low, Seri Mustafah and Anis Larbi from the SIgN Flow Cytometry team for their assistance. The authors are grateful to all patients and healthy volunteers for their participation in the study. Finally, the authors would like to thank Laurent Rénia and Insight Editing London for comments and proofreading the manuscript prior to submission. This work was supported by core research grants provided to the Singapore Immunology Network (SIgN) by the Biomedical Research Council (BMRC) and by the BMRC A*STAR-led Zika Virus Consortium Fund [project number: 15/1/82/27/001], Agency for Science, Technology and Research (A*STAR), Singapore. This work was also supported by funds provided by the Medical Research Council (MRC) [project number: MC_PC_15094], and by the HPRU in Emerging and Zoonotic Infections Cross NIHR Strategic Research Fund [project number: ZLKN_11447], United Kingdom. The views expressed are those of the author(s) and not necessarily those of the A*STAR, NHS, the NIHR, the Department of Health or PHE.

References

1. Korzeniewski, K, Juszczak, D , Zwolinska, E. Zika - another threat on the epidemiological map of the world. *Int Marit Health*. 2016;67(1):31-7.

2. Dick, GW, Kitchen, SF , Haddow, AJ. Zika virus. I. Isolations and serological specificity. *Trans R Soc Trop Med Hyg*. 1952;46(5):509-20.

3. Duffy, MR et al. Zika virus outbreak on Yap Island, Federated States of Micronesia. *N Engl J Med*. 2009;360(24):2536-43.

4. Cao-Lormeau, VM et al. Guillain-Barre Syndrome outbreak associated with Zika virus infection in French Polynesia: a case-control study. *Lancet*. 2016;387(10027):1531-9.

5. Brasil, P et al. Zika Virus Infection in Pregnant Women in Rio de Janeiro - Preliminary Report. *N Engl J Med*. 2016 doi:10.1056/NEJMoa1602412.

6. Foo, SS et al. Asian Zika virus strains target CD14+ blood monocytes and induce M2-skewed immunosuppression during pregnancy. *Nat Microbiol*. 2017 doi:10.1038/s41564-017-0016-3.

7. Lum, FM et al. Sensitive detection of Zika virus antigen in patients' whole blood as an alternative diagnostic approach. *J Infect Dis*. 2017 doi:10.1093/infdis/jix276.

8. Lum, FM et al. Zika Virus Infects Human Fetal Brain Microglia and Induces Inflammation. *Clin Infect Dis*. 2017;64(7):914-20.

9. Michlmayr, D, Andrade, P, Gonzalez, K, Balmaseda, A , Harris, E. CD14+CD16+ monocytes are the main target of Zika virus infection in peripheral blood mononuclear cells in a paediatric study in Nicaragua. *Nat Microbiol*. 2017 doi:10.1038/s41564-017-0035-0.

10. Liu, X et al. Transcriptomic signatures differentiate survival from fatal outcomes in humans infected with Ebola virus. *Genome Biol*. 2017;18(1):4.

11. Bowen, JR et al. Zika Virus Antagonizes Type I Interferon Responses during Infection of Human Dendritic Cells. *PLoS Pathog*. 2017;13(2):e1006164.

12. Carroll, MW et al. Temporal and spatial analysis of the 2014-2015 Ebola virus outbreak in West Africa. *Nature*. 2015;524(7563):97-101.

13. Dowall, SD et al. Elucidating variations in the nucleotide sequence of Ebola virus associated with increasing pathogenicity. *Genome Biol*. 2014;15(11):540.

14. Singapore Zika Study, G. Outbreak of Zika virus infection in Singapore: an epidemiological, entomological, virological, and clinical analysis. *Lancet Infect Dis*. 2017;17(8):813-21.

15. Montaldo, E et al. Human NK cell receptors/markers: a tool to analyze NK cell development, subsets and function. *Cytometry A*. 2013;83(8):702-13.

709 16. Yu, J et al. CD94 surface density identifies a functional intermediary
710 between the CD56bright and CD56dim human NK-cell subsets. *Blood*.
711 2010;115(2):274-81.

712 17. Fogel, LA, Sun, MM, Geurs, TL, Carayannopoulos, LN , French, AR.
713 Markers of nonselective and specific NK cell activation. *J Immunol*.
714 2013;190(12):6269-76.

715 18. Michel, T, Hentges, F , Zimmer, J. Consequences of the crosstalk
716 between monocytes/macrophages and natural killer cells. *Front*
717 *Immunol*. 2012;3:403.

718 19. Marcais, A et al. The metabolic checkpoint kinase mTOR is essential
719 for IL-15 signaling during the development and activation of NK cells.
720 *Nat Immunol*. 2014;15(8):749-57.

721 20. Kam, YW et al. Specific Biomarkers Associated With Neurological
722 Complications and Congenital Central Nervous System Abnormalities
723 From Zika Virus-Infected Patients in Brazil. *J Infect Dis*.
724 2017;216(2):172-81.

725 21. El Costa, H et al. ZIKA virus reveals broad tissue and cell tropism
726 during the first trimester of pregnancy. *Sci Rep*. 2016;6:35296.

727 22. Hamel, R et al. Biology of Zika Virus Infection in Human Skin Cells. *J*
728 *Virol*. 2015;89(17):8880-96.

729 23. Quicke, KM et al. Zika Virus Infects Human Placental Macrophages.
730 *Cell Host Microbe*. 2016;20(1):83-90.

731 24. Gordon, S, Pluddemann, A , Martinez Estrada, F. Macrophage
732 heterogeneity in tissues: phenotypic diversity and functions. *Immunol*
733 *Rev*. 2014;262(1):36-55.

734 25. Gordon, S , Taylor, PR. Monocyte and macrophage heterogeneity. *Nat*
735 *Rev Immunol*. 2005;5(12):953-64.

736 26. Martinez, FO, Gordon, S, Locati, M , Mantovani, A. Transcriptional
737 profiling of the human monocyte-to-macrophage differentiation and
738 polarization: new molecules and patterns of gene expression. *J*
739 *Immunol*. 2006;177(10):7303-11.

740 27. Ploeger, DT et al. Cell plasticity in wound healing: paracrine factors of
741 M1/ M2 polarized macrophages influence the phenotypical state of
742 dermal fibroblasts. *Cell Commun Signal*. 2013;11(1):29.

743 28. Italiani, P , Boraschi, D. From Monocytes to M1/M2 Macrophages:
744 Phenotypical vs. Functional Differentiation. *Front Immunol*. 2014;5:514.

745 29. Grubaugh, ND et al. Genomic epidemiology reveals multiple
746 introductions of Zika virus into the United States. *Nature*. 2017
747 doi:10.1038/nature22400.

748 30. Rodpothong, P , Auewarakul, P. Viral evolution and transmission
749 effectiveness. *World J Virol*. 2012;1(5):131-4.

750 31. Mamrut, S et al. Integrative analysis of methylome and transcriptome in
751 human blood identifies extensive sex- and immune cell-specific
752 differentially methylated regions. *Epigenetics*. 2015;10(10):943-57.

753 32. Wong, KL et al. Gene expression profiling reveals the defining features
754 of the classical, intermediate, and nonclassical human monocyte
755 subsets. *Blood*. 2011;118(5):e16-31.

756 33. Carrasco, L. The inhibition of cell functions after viral infection. A
757 proposed general mechanism. *FEBS Lett*. 1977;76(1):11-5.

758 34. Randall, RE , Goodbourn, S. Interferons and viruses: an interplay
759 between induction, signalling, antiviral responses and virus
760 countermeasures. *J Gen Virol*. 2008;89(Pt 1):1-47.

761 35. Lunemann, JD. Epstein-Barr virus in multiple sclerosis: a continuing
762 conundrum. *Neurology*. 2012;78(1):11-2.

763 36. Tucker, WG , Andrew Paskauskas, R. The MSMV hypothesis: measles
764 virus and multiple sclerosis, etiology and treatment. *Med Hypotheses*.
765 2008;71(5):682-9.

766 37. Robertson, MJ. Role of chemokines in the biology of natural killer cells.
767 *J Leukoc Biol*. 2002;71(2):173-83.

768 38. Thapa, M, Welner, RS, Pelayo, R , Carr, DJ. CXCL9 and CXCL10
769 expression are critical for control of genital herpes simplex virus type 2
770 infection through mobilization of HSV-specific CTL and NK cells to the
771 nervous system. *J Immunol*. 2008;180(2):1098-106.

772 39. Warren, HS , Smyth, MJ. NK cells and apoptosis. *Immunol Cell Biol*.
773 1999;77(1):64-75.

774 40. Kobayashi, M et al. Identification and purification of natural killer cell
775 stimulatory factor (NKSF), a cytokine with multiple biologic effects on
776 human lymphocytes. *J Exp Med*. 1989;170(3):827-45.

777 41. Liu, J et al. Interleukin-12: an update on its immunological activities,
778 signaling and regulation of gene expression. *Curr Immunol Rev*.
779 2005;1(2):119-37.

780 42. French, AR, Holroyd, EB, Yang, L, Kim, S , Yokoyama, WM. IL-18 acts
781 synergistically with IL-15 in stimulating natural killer cell proliferation.
782 *Cytokine*. 2006;35(5-6):229-34.

783 43. Takeda, K et al. Defective NK cell activity and Th1 response in IL-18-
784 deficient mice. *Immunity*. 1998;8(3):383-90.

785 44. Kastelein, RA, Hunter, CA , Cua, DJ. Discovery and biology of IL-23
786 and IL-27: related but functionally distinct regulators of inflammation.
787 *Annu Rev Immunol*. 2007;25:221-42.

788 45. Matsui, M et al. Interleukin-27 activates natural killer cells and
789 suppresses NK-resistant head and neck squamous cell carcinoma
790 through inducing antibody-dependent cellular cytotoxicity. *Cancer Res*.
791 2009;69(6):2523-30.

792 46. van de Wetering, D, de Paus, RA, van Dissel, JT , van de Vosse, E. IL-
793 23 modulates CD56+/CD3- NK cell and CD56+/CD3+ NK-like T cell
794 function differentially from IL-12. *Int Immunol*. 2009;21(2):145-53.

795 47. Kim, TJ et al. Homotypic NK cell-to-cell communication controls
796 cytokine responsiveness of innate immune NK cells. *Sci Rep*.
797 2014;4:7157.

798 48. Krylova, NV, Smolina, TP , Leonova, GN. Molecular Mechanisms of
799 Interaction Between Human Immune Cells and Far Eastern Tick-Borne
800 Encephalitis Virus Strains. *Viral Immunol*. 2015;28(5):272-81.

801 49. Gotlieb, N et al. The misleading nature of in vitro and ex vivo findings in
802 studying the impact of stress hormones on NK cell cytotoxicity. *Brain*
803 *Behav Immun*. 2015;45:277-86.

804 50. Notario, L, Alari-Pahissa, E, de Molina, A , Lauzurica, P. CD69
805 Deficiency Enhances the Host Response to Vaccinia Virus Infection
806 through Altered NK Cell Homeostasis. *J Virol*. 2016;90(14):6464-74.

807 51. Sellers, RS, Clifford, CB, Treuting, PM , Brayton, C. Immunological
808 variation between inbred laboratory mouse strains: points to consider in
809 phenotyping genetically immunomodified mice. *Vet Pathol*.
810 2012;49(1):32-43.

811 52. Cugola, FR et al. The Brazilian Zika virus strain causes birth defects in
812 experimental models. *Nature*. 2016;534(7606):267-71.

813 53. Gaucher, D et al. Yellow fever vaccine induces integrated multilineage
814 and polyfunctional immune responses. *J Exp Med*. 2008;205(13):3119-
815 31.

816 54. Morrison, BE, Park, SJ, Mooney, JM , Mehrad, B. Chemokine-
817 mediated recruitment of NK cells is a critical host defense mechanism
818 in invasive aspergillosis. *J Clin Invest*. 2003;112(12):1862-70.

819 55. Eubank, TD, Galloway, M, Montague, CM, Waldman, WJ , Marsh, CB.
820 M-CSF induces vascular endothelial growth factor production and
821 angiogenic activity from human monocytes. *J Immunol*.
822 2003;171(5):2637-43.

823 56. Kuroda, T et al. Monocyte chemoattractant protein-1 transfection
824 induces angiogenesis and tumorigenesis of gastric carcinoma in nude
825 mice via macrophage recruitment. *Clin Cancer Res*. 2005;11(21):7629-
826 36.

827 57. Marumo, T, Schini-Kerth, VB , Busse, R. Vascular endothelial growth
828 factor activates nuclear factor-kappaB and induces monocyte
829 chemoattractant protein-1 in bovine retinal endothelial cells. *Diabetes*.
830 1999;48(5):1131-7.

831 58. Conti, P et al. Activation of human natural killer cells by
832 lipopolysaccharide and generation of interleukin-1 alpha, beta, tumour
833 necrosis factor and interleukin-6. Effect of IL-1 receptor antagonist.
834 *Immunology*. 1991;73(4):450-6.

835 59. Park, JY et al. IL-15-induced IL-10 increases the cytolytic activity of
836 human natural killer cells. *Mol Cells*. 2011;32(3):265-72.

837 60. Metcalfe, SM. LIF in the regulation of T-cell fate and as a potential
838 therapeutic. *Genes Immun*. 2011;12(3):157-68.

839 61. Wolk, K, Kunz, S, Asadullah, K , Sabat, R. Cutting edge: immune cells
840 as sources and targets of the IL-10 family members? *J Immunol*.
841 2002;168(11):5397-402.

842 62. Zhang, Q, Putheti, P, Zhou, Q, Liu, Q , Gao, W. Structures and
843 biological functions of IL-31 and IL-31 receptors. *Cytokine Growth*
844 *Factor Rev*. 2008;19(5-6):347-56.

845 63. Elong Ngono, A et al. Mapping and Role of the CD8+ T Cell Response
846 During Primary Zika Virus Infection in Mice. *Cell Host Microbe*.
847 2017;21(1):35-46.

848 64. Kerdiles, Y, Ugolini, S , Vivier, E. T cell regulation of natural killer cells.
849 *J Exp Med*. 2013;210(6):1065-8.

850 65. Baronti, C et al. Complete coding sequence of zika virus from a French
851 polynesia outbreak in 2013. *Genome Announc*. 2014;2(3).

852 66. Balm, MN et al. A diagnostic polymerase chain reaction assay for Zika
853 virus. *J Med Virol*. 2012;84(9):1501-5.

854 67. Wu, D et al. Chikungunya outbreak in Guangdong Province, China,
855 2010. *Emerging infectious diseases*. 2012;18(3):493-5.

856 68. Bosworth, A et al. A comparison of host gene expression signatures
857 associated with infection in vitro by the Makona and Ecran (Mayinga)
858 variants of Ebola virus. *Sci Rep*. 2017;7:43144.

859 69. Tang, H et al. Zika Virus Infects Human Cortical Neural Progenitors
860 and Attenuates Their Growth. *Cell Stem Cell*. 2016;18(5):587-90.

70. Kim, D et al. TopHat2: accurate alignment of transcriptomes in the presence of insertions, deletions and gene fusions. *Genome Biol*. 2013;14(4):R36.

71. Langmead, B , Salzberg, SL. Fast gapped-read alignment with Bowtie 2. *Nat Methods*. 2012;9(4):357-9.

72. Robinson, MD, McCarthy, DJ , Smyth, GK. edgeR: a Bioconductor package for differential expression analysis of digital gene expression data. *Bioinformatics*. 2010;26(1):139-40.

73. Saeed, AI et al. TM4: a free, open-source system for microarray data management and analysis. *Biotechniques*. 2003;34(2):374-8.

74. Beerenwinkel, N , Zagordi, O. Ultra-deep sequencing for the analysis of viral populations. *Curr Opin Virol*. 2011;1(5):413-8.

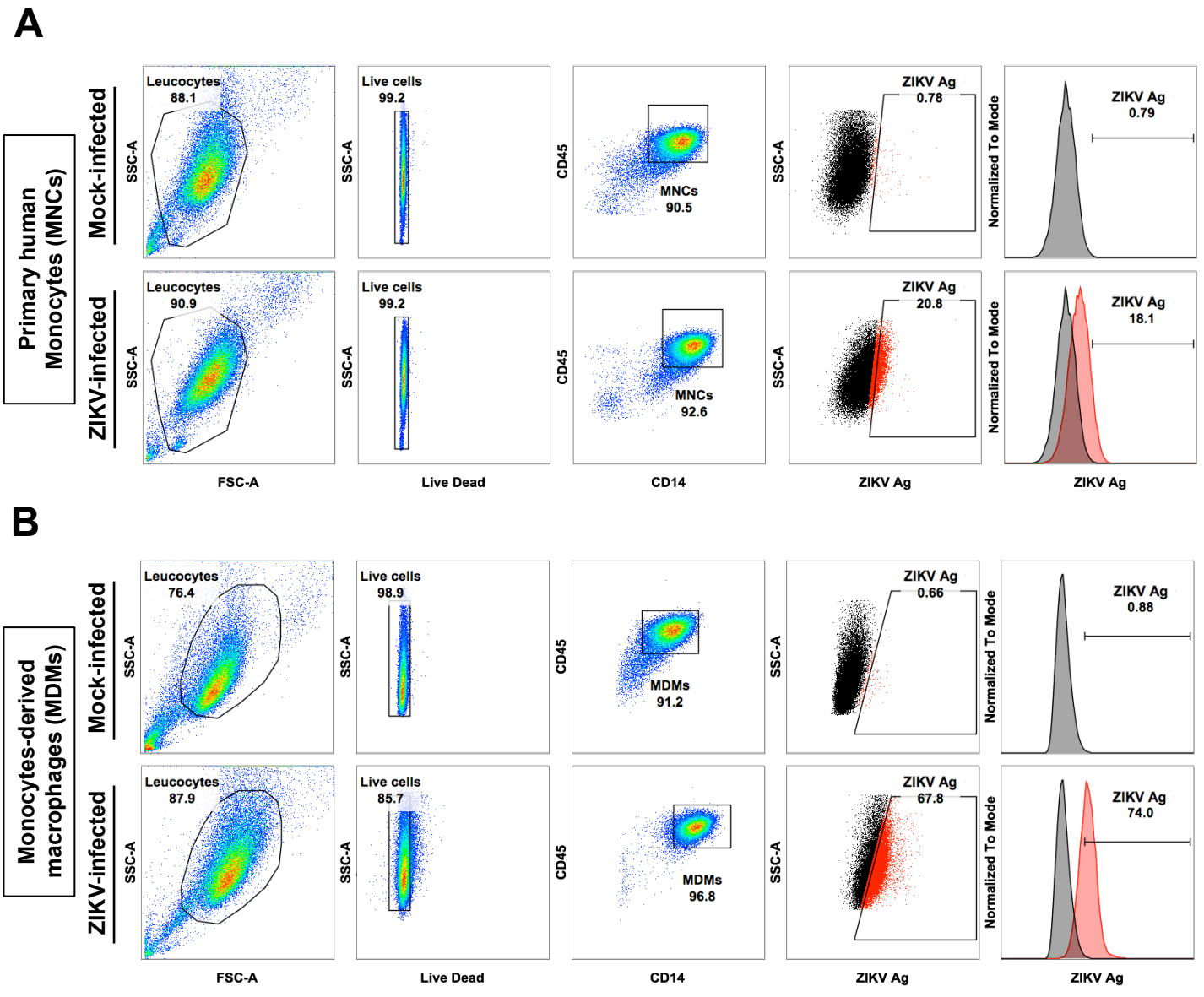

Figure 1: Primary human MNCs and MDMs are targets of ZIKV infection. Isolated human primary MNCs and MDMs (2×10^6 cells each) were infected with ZIKV at MOI 10 and harvested at 24 and 72 hpi. Flow cytometry gating on (**A**) monocytes (MNCs) and (**B**) MDMs. Gating for positive infection was set using the mock-infected samples. For the dot plots, cells positive for ZIKV Ag are shown in red. For the histogram, ZIKV-infected samples (red) were overlaid on mock-infected samples (black). Compiled results for (**C**) infection (ZIKV Ag) and (**D**) viral load detected in MNCs and MDMs obtained from five healthy donors. All data are presented as mean ± SD. *$P < 0.05$, by Mann Whitney *U* test, two tailed. Viral load data was not statistically significant between 24 and 72 hpi in MNCs by Mann Whitney *U* test, two tailed. Abbreviations: hpi, hours post-infection; MDM, monocyte-derived macrophage; MNC, monocyte; ZIKV, Zika virus; Ag, antigen.

Figure 1_Lum et al., 2017

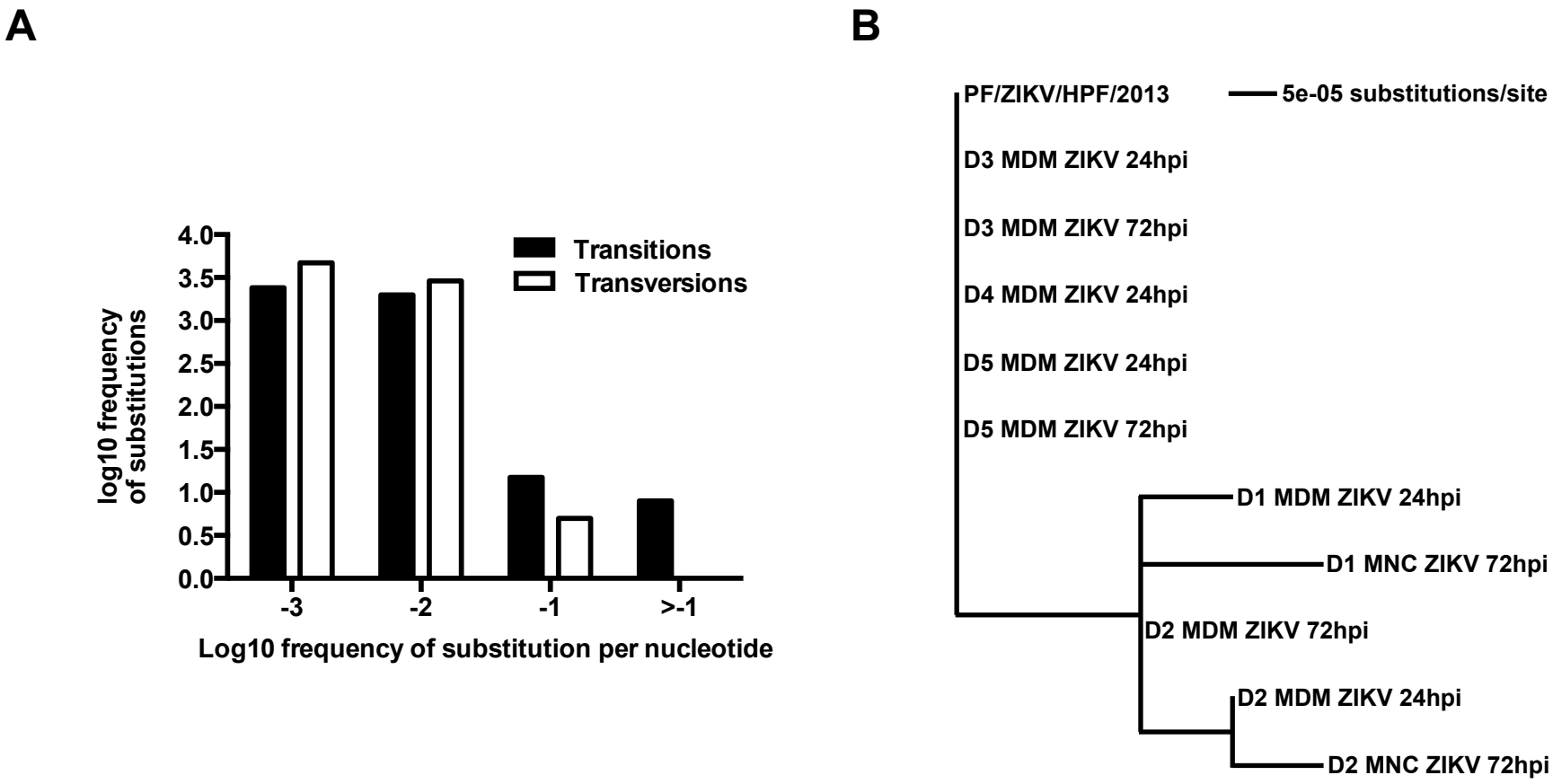

Figure 2: Phylogenetic analyses based on sample consensus sequences. (**A**) Frequency of ZIKV minor variants (transitions and transversions) recovered from infected human primary MNCs and MDMs isolated from five donors. Bin -3 is where ≤1/1000 reads show a specific change at an individual nucleotide position. Bin -2 is >1/1000 and ≤1/100 reads showing a difference. Bin -1 is >1/100 and ≤1/10 reads and Bin > -1 is >1/10 reads showing a change up to a logical limit of just under ½. (**B**) Phylogenetic tree generated from the alignment of consensus sequences of ZIKV RNA recovered from the same samples as described in (**A**). All samples included in the tree had a mean sequence coverage >10 at each nucleotide position. PF/ZIKV/HPF/2013 is the virus strain used for infection and denoted as the reference sample in this analysis. Abbreviations: hpi, hours post-infection; MDM, monocyte-derived macrophage; MNC, monocyte; ZIKV, Zika virus.

Figure 2_Lum et al., 2017

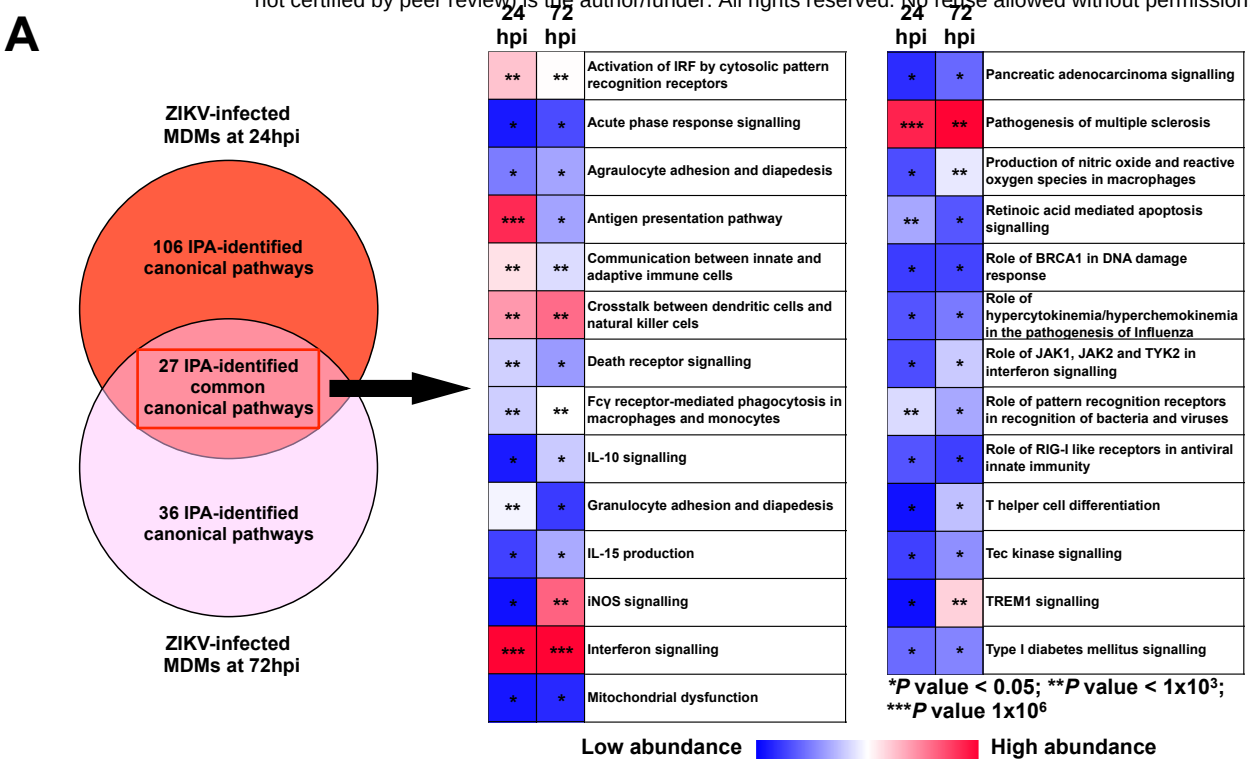

Figure 3: Transcriptomic profiling of host cells during ZIKV infection. Primary human MNCs and MDMs (2×10^6 cells per infection) were infected with ZIKV at MOI 10 and harvested at 24 and 72 hpi for transcriptomic analysis by RNA-seq and then compared to mock-infected controls. (**A**) Venn-diagram illustrating the proportion of up-regulated signaling pathways identified by IPA in ZIKV-infected MDMs. Up-regulation intensity of the 27 common canonical pathways are shown in a heat-map. Stars within the boxes represent the calculated *P* values associated with each identified pathway, compared to the mock-infected samples. (**B**) The five most up-regulated genes within the top three signaling pathways at 24 and 72 hpi are shown: Interferon pathway, multiple sclerosis pathway and crosstalk between moDCs and NK cells. Data presented were obtained from a total of five donors. Abbreviations: hpi, hours post-infection; NK, natural killer; IPA, ingenuity pathway analysis; MDM, monocyte-derived macrophage; MNC, monocyte; moDCs, monocyte-derived dendritic cells; ZIKV, Zika virus.

Figure 3_Lum et al., 2017

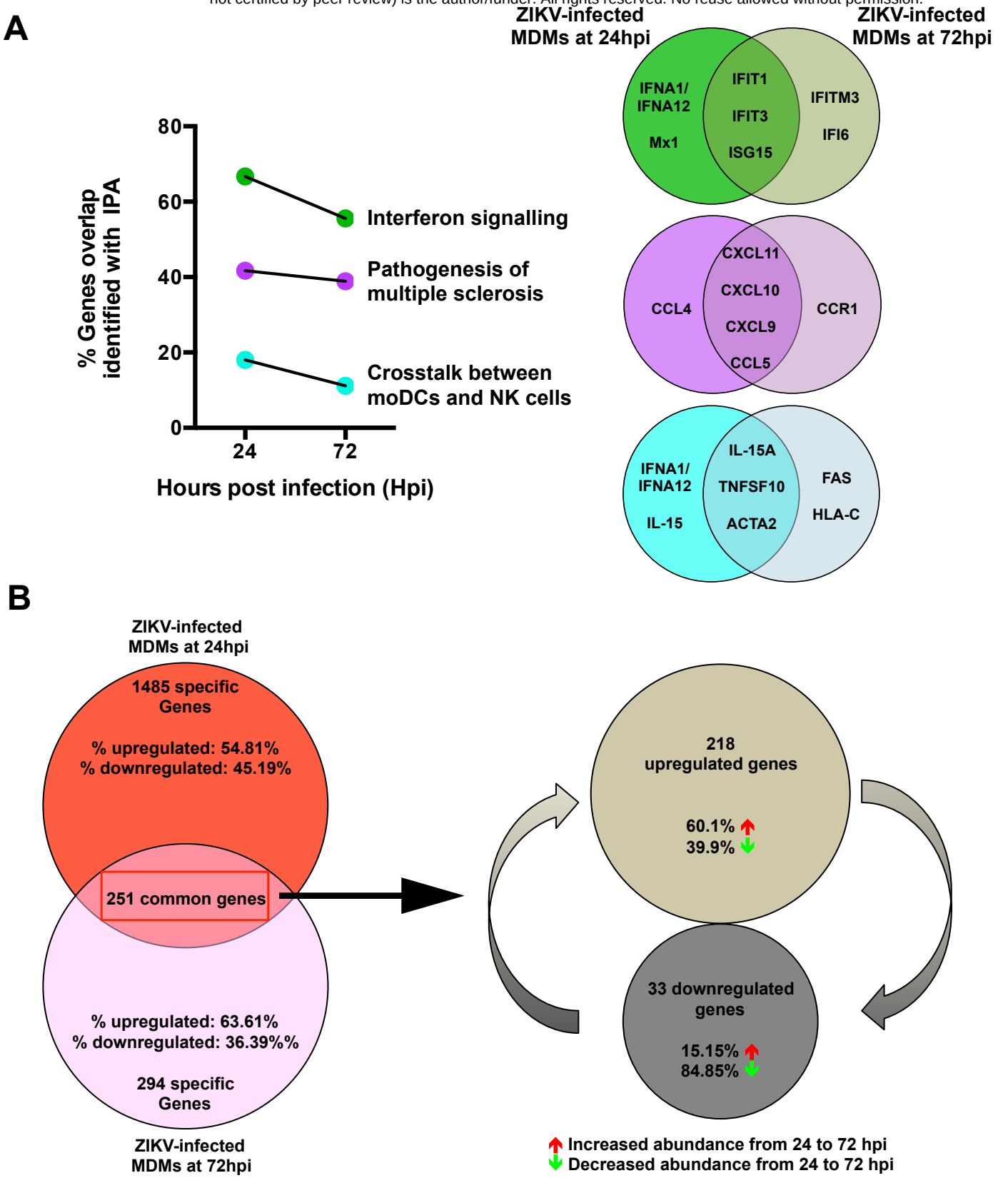

Figure 4: Transition of the host cellular response over the course of ZIKV infection. The host cellular response was analyzed and investigated by RNA-sequencing and significant transcriptomic differences were identified. (**A**) Transitional analysis (% genes overlapping) of the top three common canonical signaling pathways was determined using IPA of infected MDMs. Venn diagrams indicate the top five common and time-point specific genes associated with each canonical pathway. (**B**) Proportion of common and differentially expressed genes within ZIKV-infected MDMs at 24 and 72 hpi. Data presented were obtained from a total of five donors. Abbreviations: moDCs, monocyte-derived dendritic cells; hpi, hours post-infection; IPA, ingenuity pathway analysis; ZIKV, Zika virus; MDM, monocyte-derived macrophage.

Figure 4_Lum et al., 2017

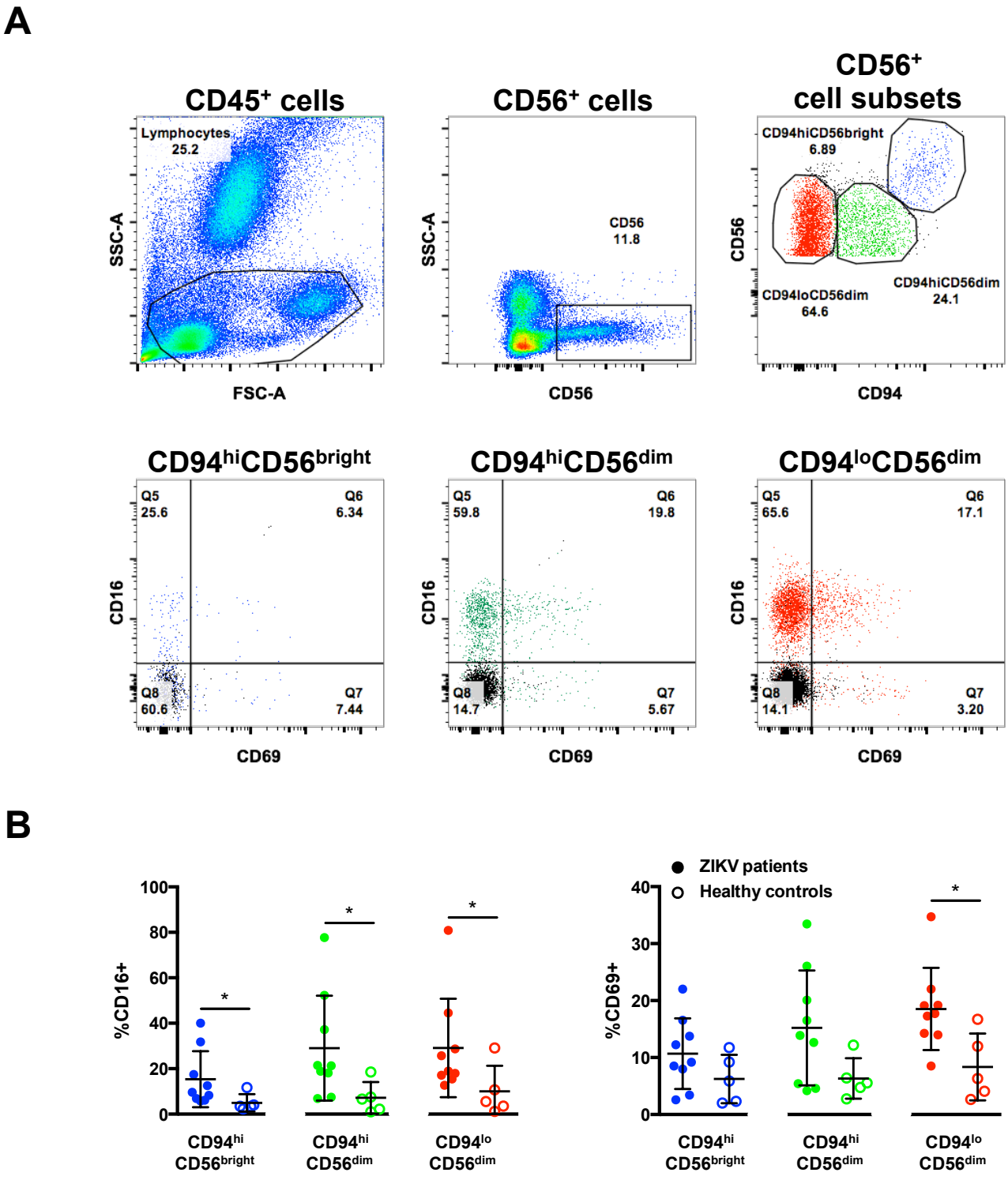

Figure 5: Activation of CD56⁺ cells in patients infected with ZIKV. (**A**) Gating strategy of CD56⁺ cell subsets and their expression of CD16 and CD69. CD56⁺ cells were first gated from CD45⁺ lymphocytes from peripheral blood mononuclear cells isolated from patients. These populations were further gated into three populations based on the expression of surface marker CD94: CD94hiCD56bright cells (blue), CD94hiCD56dim (green) and CD94loCD56dim (red). The data presented correspond to a representative patient infected with ZIKV. Cells from a healthy control are overlaid and depicted as the black population (Q8). (**B**) Compiled data on the percentage of gated subsets that are positive for CD16 (Q5 and Q6) and CD69 (Q6 and Q7). Patients (n=9) are depicted as filled circles, and healthy controls (n=5) are depicted as clear circles. All data are presented as mean ± SD. *$P < 0.05$, by Mann Whitney *U* test, two tailed. Abbreviations: NK, natural killer; ZIKV, Zika virus.

Figure 5_Lum et al., 2017

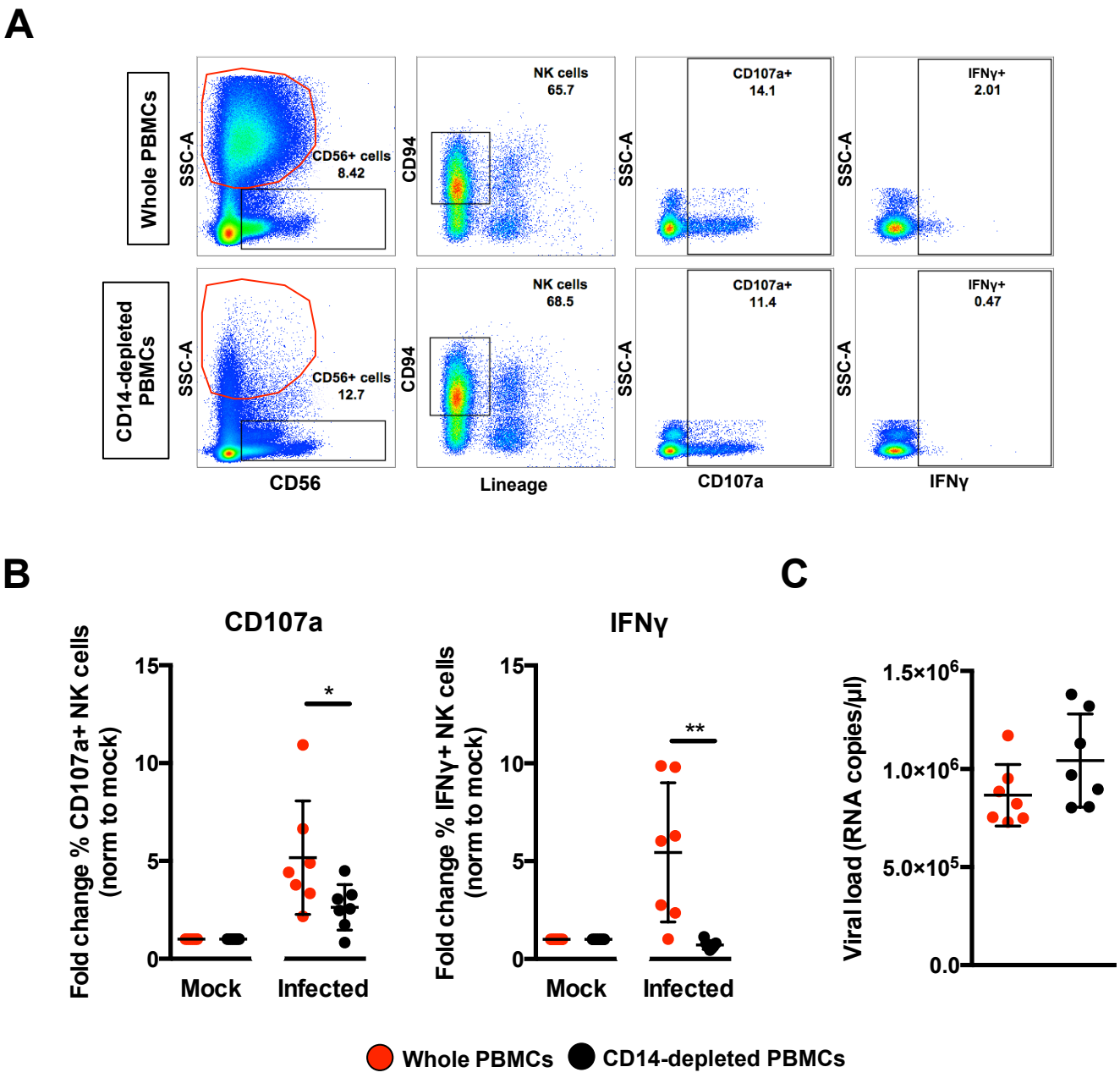

Figure 6: Role of monocytes in NK-cell activity. Full PBMCs and CD14-depleted PBMCs (2×10^6 cells per infection) were infected with Zika virus (ZIKV) at MOI 10 and harvested at 36 hpi. (**A**) Gating strategy of $CD94^+CD56^+Lineage^-$ NK cells and their expression of CD69, CD107a and IFNγ. Plots from one representative donor are shown. The red circle indicates the presence or absence of $CD14^+$ monocytes. (**B**) Compiled percentages of CD107a and IFNγ-positive NK cells (depicted in (**A**)) as normalized to the respective mock sample. (**C**) Viral load in the infected cells. Data shown were derived from seven donors. Lineage markers CD3, CD19, CD20 and CD14 have been included to rule out the presence of non-NK cells. All data are presented as mean ± SD. *$P < 0.05$, **$P < 0.01$, by Mann Whitney *U* test, two tailed. Viral load data was not statistically significant between the two conditions by Mann Whitney *U* test, two tailed. Abbreviations; NK, natural killer; PMBC, peripheral blood mononuclear cell; hpi, hours post-infection.

Figure 6_Lum et al., 2017

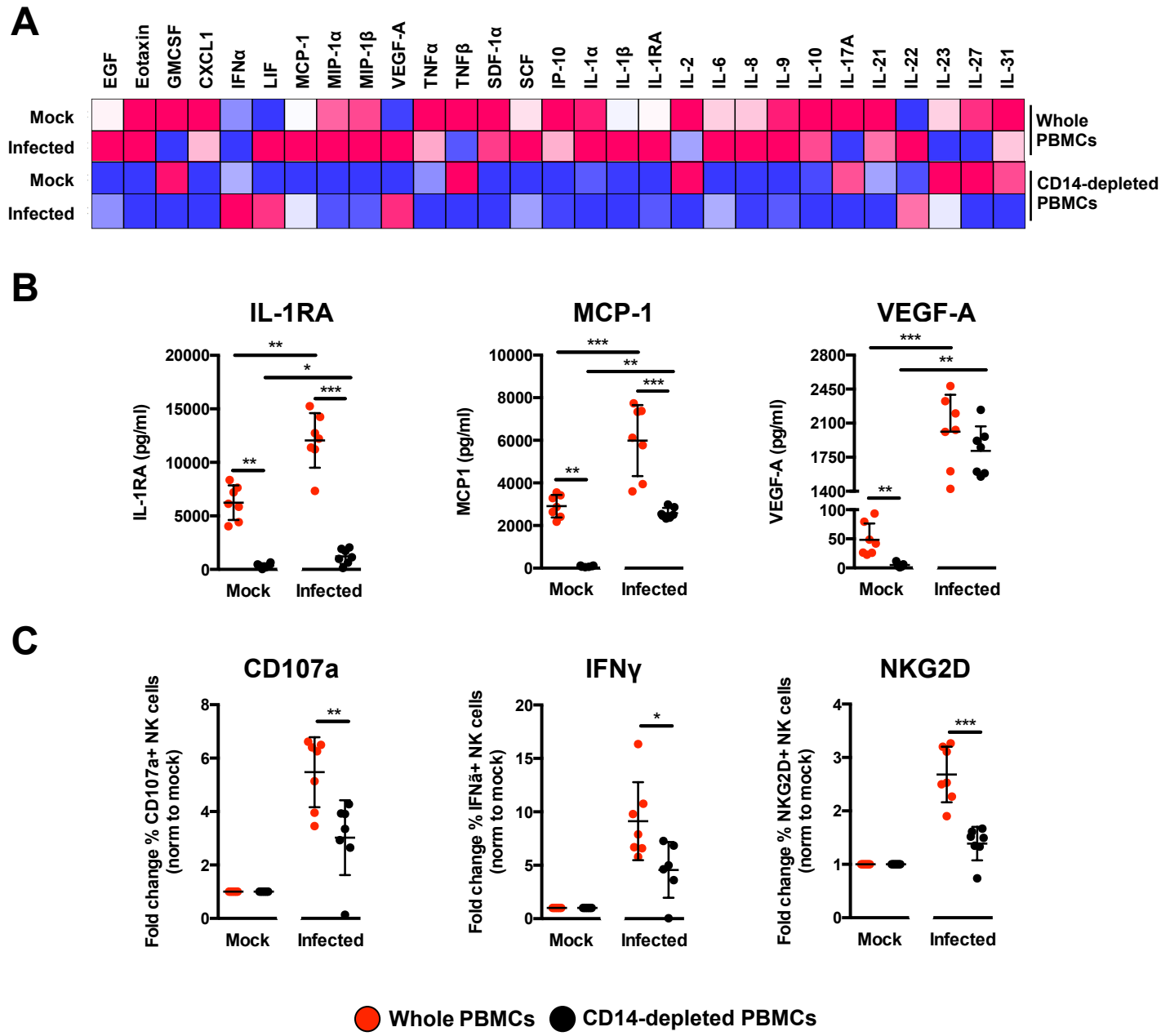

Figure 7: Immune profiling of ZIKV-infected PBMCs. (**A**) Immune mediators in the culture supernatant of ZIKV-infected PBMCs and CD14-depleted PBMCs were quantified with a 45-plex microbeads assay. Concentrations were scaled between 0 and 1. (**B**) Bar-charts of three cytokines, which levels were significantly affected by both the depletion of $CD14^+$ monocytes and ZIKV infection. (**C**) Stimulatory capacity of the culture supernatants were further evaluated with freshly isolated PBMCs. Culture supernatant was added in a ratio of 1:10 and cells were harvested at 36 hours post-stimulation. Compiled percentages of CD107a, IFNγ, and NKG2D-positive $CD94^+CD56^+$ NK cells are shown as normalized to the respective mock sample. Data displayed were derived from seven donors. Lineage markers CD3, CD19, CD20 and CD14 have been included to rule out the presence of non-NK cells. All data are presented as mean ± SD. $^*P < 0.05$, $^{**}P < 0.01$, $^{***}P < 0.001$, by Mann Whitney *U* test, two tailed. Abbreviations: NK, natural killer; PMBC, peripheral blood mononuclear cell.

Figure 7_Lum et al., 2017

Table 1: Summary of nucleotide differences at specific genome positions

Position in consensus sequence[A]	Nucleotide difference	Sample(s)	
1904	g → a	D1 MNC ZIKV 72hpi	
2673	t → c	D2 MDM ZIKV 24hpi	D2 MNC ZIKV 72hpi
2815	t	D1 MDM ZIKV 24hpi D2 MDM ZIKV 72hpi D2 MNC ZIKV 72hpi	D2 MDM ZIKV 24hpi D1 MNC ZIKV 72hpi
	c	D3 MDM ZIKV 24hpi D4 MDM ZIKV 24hpi D5 MDM ZIKV 72hpi	D3 MDM ZIKV 72hpi D5 MDM ZIKV 24hpi PF/ZIKV/HPF/2013
4211	a	D3 MDM ZIKV 24hpi D4 MDM ZIKV 24hpi D5 MDM ZIKV 72hpi	D3 MDM ZIKV 72hpi D5 MDM ZIKV 24hpi PF/ZIKV/HPF/2013
	g	D1 MDM ZIKV 24hpi D2 MDM ZIKV 72hpi D2 MNC ZIKV 72hpi	D2 MDM ZIKV 24hpi D1 MNC ZIKV 72hpi
10253	t → c	D1 MDM ZIKV 24hpi	D2 MNC ZIKV 72hpi
10472	t → c	D1 MNC ZIKV 72hpi	

The phylogenetic tree shown in Figure 3B revealed specific nucleotide differences at 6 different positions within the consensus sequence. All samples included had a mean coverage of greater than 10. PF/ZIKV/HPF/2013 represents the virus used for the infection and therefore, denoted as the reference sample in this analysis. Abbreviations: MNC, monocytes; MDM, monocyte-derived macrophage. [A]Note that minor variant file numbering of positions starts at 0 rather than 1.

Table 2: Selected nucleotide positions from the minor variants file of the inoculum

Position in consensus sequenceA	Frequency of minor nucleotide variants				
	A	C	G	T(U)	D (A/G/T)
1904	0.11324	0	0.88601	0.00074	0
2673	0.00681	0.11779	0.000619	0.87476	0
2815	0.00876	0.64463	0	0.34659	0
4211	0.65122	0	0.34815	0.000626	0
10253	0.000891	0.11229	0	0.8868	0
10472	0.00108	0.00543	0.00108	0.99239	0

Table showing the frequency distribution of minor nucleotide variants at six positions in the consensus sequence. Major variant (i.e. the consensus nucleotide) at each position is indicated by the nucleotide with the highest frequency. [A]Note that minor variant file numbering of positions starts at 0 rather than 1.